NASA CONTRACTOR REPORT

NASA CR-776

NASA CR-776

DRAG COEFFICIENTS OF MICROSCOPIC SPHERES IN FREE-MOLECULE FLOW

by A. S. Hersh, J. F. Friichtenicht, and J. C. Slattery

Prepared by
TRW SYSTEMS
Redondo Beach, Calif.
for

NATIONAL AERONAUTICS AND SPACE ADMINISTRATION • WASHINGTON, D. C. • MAY 1967

NASA-CR-776

DRAG COEFFICIENTS OF MICROSCOPIC SPHERES IN FREE-MOLECULE FLOW

By A. S. Hersh, J. F. Friichtenicht, and J. C. Slattery

Prepared under Contract No. NASw-1336 by
TRW SYSTEMS
Redondo Beach, Calif.

for

NATIONAL AERONAUTICS AND SPACE ADMINISTRATION

For sale by the Clearinghouse for Federal Scientific and Technical Information
Springfield, Virginia 22151 – CFSTI price $3.00

PRECEDING PAGE BLANK NOT FILMED.

DRAG COEFFICIENTS OF MICROSCOPIC SPHERES IN FREE-MOLECULE FLOW*

by A. S. Hersh, J. F. Friichtenicht, and J. C. Slattery

ABSTRACT

The "free flight" technique has been utilized to determine average drag coefficients C_D for microscopic spherical iron particles in free-molecule flow ($K_n >> 1$). Particles ranging in velocity from about 0.5 to 3.5 km/sec were obtained from an electrostatic particle accelerator. For an air background gas, the flight speed ratio extends from the nonhyperthermal regime ($S_{min} \approx 1$) well into the hyperthermal region ($S_{max} \approx 9$). In this regime, C_D for spheres is relatively sensitive to the details of atom-surface interactions and precise measurements of C_D provide a basis for inferring characteristics of these interactions. The experimental results were compared to the free-molecule models of Schamberg and Schaaf-Chambre. The Schamberg model gives a better representation of the experimental data, but significant deviations are noted at low speed ratios. The discrepancy has been attributed to variations in accommodation coefficient, α, and type of re-emission (i.e., specular or diffuse) with speed ratio. Following modification of Schamberg's model, the type of re-emission required to force a fit to the experimental data was evaluated by assuming Epstein's model for the variation of α with S. It was concluded that the atom-surface collisions range from specular at large S to nearly completely diffuse for small S. Although the results are not unambiguous, they do give a plausible representation of the experimentally derived data.

---

*This work supported by the NASA under Contract NASw-1336.

1. INTRODUCTION

In spite of the fact that extensive studies of aerodynamic flow problems have been conducted by a variety of techniques, it is still not possible to predict accurately the drag force acting on spheres in free-molecule flow for arbitrary conditions. In the free-molecule regime, which is characterized by large Knudsen (K_n is the ratio of molecular mean free path to a typical body dimension), the drag force is due to the integrated effects of individual atom-surface collisions. By considering details of the atom-surface interactions, maximum and minimum values of the drag coefficient can usually be specified. For many applications, the extremes are sufficiently close together to justify the use of a mean value. In some applications, for example satellite drag, more precise information would be desirable. Also, at low flight speed ratios (the speed ratio S is defined as the ratio of body velocity to the most probable velocity of the gas molecules) the drag coefficient is a relatively strong function of velocity and is quite sensitive to the details of the atom-surface interactions. The results of the investigation described in this report apply primarily to the latter case.

Experimental measurements of sphere drag for large K_n using low-density wind-tunnels prove to be quite difficult because of the operating characteristics of such tunnels. In particular, very small spheres must be used to achieve the proper flow conditions and the support structure often produces major effects. To avoid these problems, the "free flight" ballistic range technique has been utilized to determine drag coefficients for microscopic spherical iron particles in the range $12 < K_n < 190$. The free flight technique has been implemented by injecting high velocity particles from an electrostatic accelerator into a gaseous target and measuring the deceleration of the particle. Particle velocities covered the range from about 0.5 to 3.5 km/sec which, for air, corresponds to speed ratios ranging from about one to nine.

The experimental results have been compared with the analytical models of Schamberg[1] and Schaaf and Chambre.[2] By assuming certain quantities, the theoretical models are in fairly good agreement with the experimental results except for some deviation at low speed ratios. In an attempt to improve the agreement, Schamberg's hyperthermal model has been modified so as to be valid at all speed ratios. It has been shown that the deviation noted is compatible with a variation in thermal accommodation coefficient as theoretically predicted by Epstein.[3]

2. EXPERIMENTAL APPARATUS AND TECHNIQUES

2.1 THE ELECTROSTATIC PARTICLE ACCELERATOR

The unique features of this experiment are due principally to the method by which the particles are accelerated and analyzed. The high velocity particles were obtained from an electrostatic particle accelerator.[4] In this device, spherical iron particles are charged electrically by a process described elsewhere[5] and are injected into the accelerating tube of a 2-million-volt Van de Graaff accelerator. The final velocity achieved by a particle is given by $v = (2\ qV/m)^{1/2}$ where q is the charge on the particle in coulombs, V is the accelerating potential in volts, m is the particle mass in kilograms, and v is the velocity measured in meters per second. The quantity q is proportional to the surface area of the particle and m is proportional to its volume; hence, q/m is proportional to the reciprocal of particle radius. Thus, the final velocity is inversely proportional to the square root of the particle radius. For the present experiment the range in particle radii is from 3 microns at 0.5 km/sec to about 0.5 micron at 3.5 km/sec.

In practice, the velocity and charge of each particle from the accelerator is measured by means of electronic detectors. For purposes of illustration consider a detector consisting of cylindrical drift tube with capacitance C connected to a high input impedance amplifier. A charged particle passing through the cylinder along its axis induces a voltage pulse of magnitude V_o given by $V_o = q/C$. The duration of the pulse is the time required by the particle to traverse the length of the cylinder. Thus, the measurement of pulse amplitude and duration yields the particle charge and velocity respectively. Given the accelerating voltage V, the mass of the particle can be calculated from the relationship given in the preceding paragraph. Depending upon the requirements of a particular experiment, several such detectors are used. Although they may perform different functions, the detectors all work on the same general principle.

2.2 EXPERIMENTAL REQUIREMENTS

The drag coefficient C_D is defined by

$$\frac{dv}{dt} = - \frac{C_D \, A\rho v^2}{2m} \tag{1}$$

where dv/dt is the deceleration of the body, v is the velocity, A and m are the projected area and mass of the body, respectively, and ρ is the mass density of the medium. Integrating Eq. (1) gives

$$\frac{1}{v} = \left(\frac{C_D \, A\rho}{2m}\right) t + \frac{1}{v_o} \tag{2}$$

or

$$\frac{dx}{dt} = \frac{1}{\left[\frac{C_D \, A\rho}{2m}\right] t + \frac{1}{v_o}} \tag{3}$$

where v_o is the velocity at t = 0 and x is the position coordinate measured along the trajectory of the particle. Integrating again and evaluating from x = 0 to $x = x_1$ gives

$$x_1 = \frac{1}{\left[\frac{C_D \, A\rho}{2m}\right]} \ln \left[\left(\frac{C_D \, A\rho}{2m}\right) v_o \, \tau_1 + 1\right] \tag{4}$$

where τ_1 is the time required for the particle to traverse the distance from x = 0 to $x = x_1$. Defining the new variables

$$y = \left(\frac{C_D\ A\rho}{2m}\right)\ x_1 \tag{5}$$

and

$$k = \frac{v_o\ \tau_1}{x_1} \tag{6}$$

and rearranging Eq. (4) gives

$$k = \frac{e^y - 1}{y} \quad . \tag{7}$$

This expression can be expanded in a Taylor series around k = 1 and the result is:

$$y = 2(k-1) - \frac{4}{3}\ (k-1)^2 + \frac{10}{9}\ (k-1)^3 - \frac{136}{135}\ (k-1)^4 + \ldots. \tag{8}$$

The series is valid for $0 < k < 2$, and, since it alternates in sign, the error is always less than the last term used.

It can be seen that k is the ratio of the initial velocity to the average velocity v_a over the interval from $x = 0$ to $x = x_1$. Thus C_D can be determined by injecting particles of known velocity and mass into a gas target of known pressure, measuring the average velocity over a known distance in the gas target, and calculating C_D from Eq. (8). However, certain precautions must be taken in applying this technique. In the preceding derivation it is tacitly assumed that the drag coefficient is constant which is not necessarily the case in regions where C_D is a strong function of velocity. At low velocities particularly, the deceleration over the measurement range should be kept small. Another factor which must be considered is collisional heating of the particle. The energy of atoms reemitted from a surface following collision is a function of the temperature of the surface and, thus, the drag coefficient is generally a function of the temperature of the body. Heating is most severe at higher velocities where C_D is nearly constant. Hence the total deceleration should be kept reasonably small in this velocity regime, also.

Now small deceleration implies that the average velocity in the gas is near the initial velocity and that k is near unity. Under these circumstances, the quantity k-1 is small and errors in the measurement of v_o or v_a are magnified. For example, assume that the ratio of v_o to v_a is known to $\pm$ 0.15% (which is typical of the actual experiment). The quantity k-1 is known to the same accuracy. For example, if $k = v_o/v_a = 1.100$, the quantity k-1 is known to $\pm$ 1.5%, but the particle is decelerated by about 18%. For a deceleration of 3%, we get $k-1 = 0.015 \pm 0.0015$ which corresponds to a possible error in C_D of about 10% due only to random errors in the measurement of the velocity ratio. The magnitude of the possible error in C_D due to excessive deceleration is dependent upon the initial velocity and cannot be evaluated as precisely as the other case. However, it is clear that the possible error in C_D is greater for the small deceleration case, so in the final reduction of the data, only those cases where $k > 1.050$ were retained.

2.3 EXPERIMENTAL APPARATUS

The apparatus used to accomplish the experimental measurements is illustrated schematically in Figure 1. In essence it consists of two time-of-flight ranges; one to establish the initial velocity and the other to measure the average velocity of the particle in the gas target region. The functions of the various components are described more fully in the following paragraphs.

The size range of particles used in the accelerator is quite large, extending from about 0.1 micron to 6.0 microns in diameter, and only a small fraction of the particles from the accelerator are compatible with a given set of experimental conditions. To avoid the task of acquiring and then rejecting data from unsatisfactory events, particles from the accelerator first pass through a particle parameter selection system. The function of this system, which has been described in some detail elsewhere,[6] is to select particles whose mass and velocity lie within specified ranges. Selected particles are allowed to enter the velocity measurement range

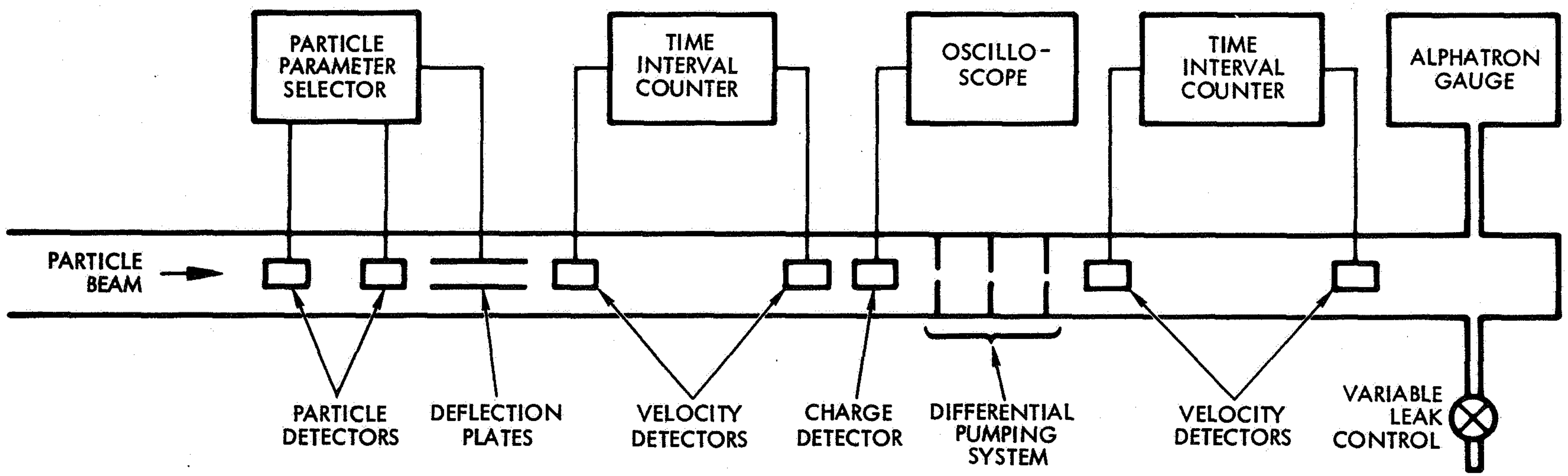

Figure 1. Schematic Diagram of the Experimental System.

while all others are deflected from the experiment. The system consists of two particle detectors similar to those described previously, an electronic logic circuit, and an electrostatic deflector. The deflector consists of a pair of parallel plates one on either side of the particle beam axis. In the quiescent state, a high voltage is applied across the plates and particles entering the region between the plates are deflected from their initial trajectory. When an acceptable particle appears, the logic circuit produces a trigger pulse which removes the voltage from the plates for a brief period of time, thereby permitting the selected particle to pass through the deflector unperturbed.

As mentioned earlier, the precise measurement of particle velocity is particularly essential in this experiment. The initial velocity is determined by means of a time-of-flight range consisting of two charged particle detectors separated by a distance of 60 cm. Signals from the two detectors are fed to identical discriminator circuits and the outputs from the discriminators are used to gate a 10 megacycle time interval counter. The counter is started by the signal originating from the first detector and the count is terminated by the signal from the second detector. A second time-of-flight range identical to the first except for a difference in length (50 cm vs. 60 cm) is installed in the gas target region. The average velocity of the decelerating particle is obtained from the second time-of-flight range.

The transit time in both of the ranges is measured to an accuracy of $\pm$ 0.1 microseconds because of the digital nature of the counters. In addition, slight differences in triggering level of the discriminators and uncertainty in the absolute length of the time-of-flight ranges also contribute to possible errors in the velocity measurements. The overall precision of the velocity ratio measurement was determined experimentally by obtaining velocity ratio measurements with the target chamber at high vacuum. It was found that the ratio of velocities is $1 \pm .0015$.

In order to measure particle charge q, an accurately calibrated charge detector is placed immediately following the first time-of-flight range. The signal from this detector is displayed on an oscilloscope and photographed for later analysis. In order to increase the precision of the pulse height measurement, the signal is added algebraically to a DC reference voltage supplied in a Type Z Tektronix preamplifier. The use of this technique permits the top of the pulse to be displayed on a very sensitive scale. It is estimated that the probable error in pulse height measurement is better than + 1%.

The particles are introduced into the target region by injecting them through the channels separating the pumping chambers of a two stage differential pumping system. The differential pumping system will support a target pressure of about 5 Torr without appreciably affecting the main accelerator vacuum which is nominally 10^{-5} Torr. One of the intermediate chambers is continuously evacuated by a 2-inch oil diffusion pump while the other is pumped by a high capacity mechanical fore pump. The starting point of the time-of-flight range is located about 2 cm downstream from the end of the differential pumping system. The deceleration suffered by the particle in traversing the low pressure chamber of the differential system is negligible, but the pressure in the other chamber is high enough to require a slight correction to the measured deceleration. The correction is made by adding a small increment of length to the 2 cm distance mentioned above and taking into account the time required by the particle to traverse this distance.

The pressure in the target chamber was adjusted by means of a precision variable leak and was continuously monitored by an Alphatron ionization gauge equipped with a digital read out. The ionization gauge was calibrated on an absolute basis over the entire operating range by means of a McLeod gauge standard. The pressure in the high pressure chamber of the differential pumping system was monitored by a Pirani gauge. The precision of the final result is not very dependent upon the accuracy of the Pirani gauge since the information from it is used only to make a minor correction of the deceleration measurement. The accuracy of the final result, on the other hand, is directly effected by the accuracy of the Alphatron gauge. It is estimated that the absolute accuracy of the pressure measurement is good to ± 1% while the results of one measurement compared to another is much better than that.

The particles used in this experiment are carbonyl iron spheres obtained from the General Aniline Food and Dyestuff Corporation. The particles are condensed from a vapor phase of carbonyl iron $Fe(CO)_4$ and are 98% pure iron with the principal impurity being carbon. The surface conditions of the particle are unknown, but, since no attempt was made to especially prepare the surface, it is assumed that it must be oxidized. An electron micrograph of the particles shown in Figure 2 indicate that most of the particles are fairly well defined spheres. A few of them, however, are slightly elongated. There is no direct method of determining the shape of a particular particle and the results obtained with all particles have been retained. The departure from sphericity of some particles may account for some of the scatter in the final results. In spite of this problem, however, the most probable shape is spherical and it is assumed that the average value of C_D over a small velocity increment is compatible with the spherical shape.

2.4 EXPERIMENTAL RESULTS

The information derived from each event is sufficient to calculate the drag coefficient by means of Eq. (8) after necessary corrections have been made. The results of the measurements of drag coefficients for iron particles in air are shown in Figure 3. The abscissa represents the average velocity of the particle in the gas target region. For these data the Knudsen number ranges from 12 to 190 which is well within the free molecule flow regime. The temperature increase of the particles due to collisional heating was estimated by assuming a heat transfer coefficient of unity. The maximum temperature reached by any given particle was less than 1000°K with many of them reaching a final temperature of less than 500°K. When required for calculational purposes the mean temperature was taken as $\sim$ 450°K.

All of the data regardless of precision is displayed in Figure 3. The scatter in the data points is due principally to the random errors which were discussed earlier. The biggest source of error is due to the measurement of the velocity ratio. Random errors associated with the measurement of target pressure and particle mass also contribute but they are relatively small. The shape of the particle can produce scatter in the measured values of C_D. More difficult to assess are the effects of non-constant body temperature and the effect of finite deceleration in a region of rapidly

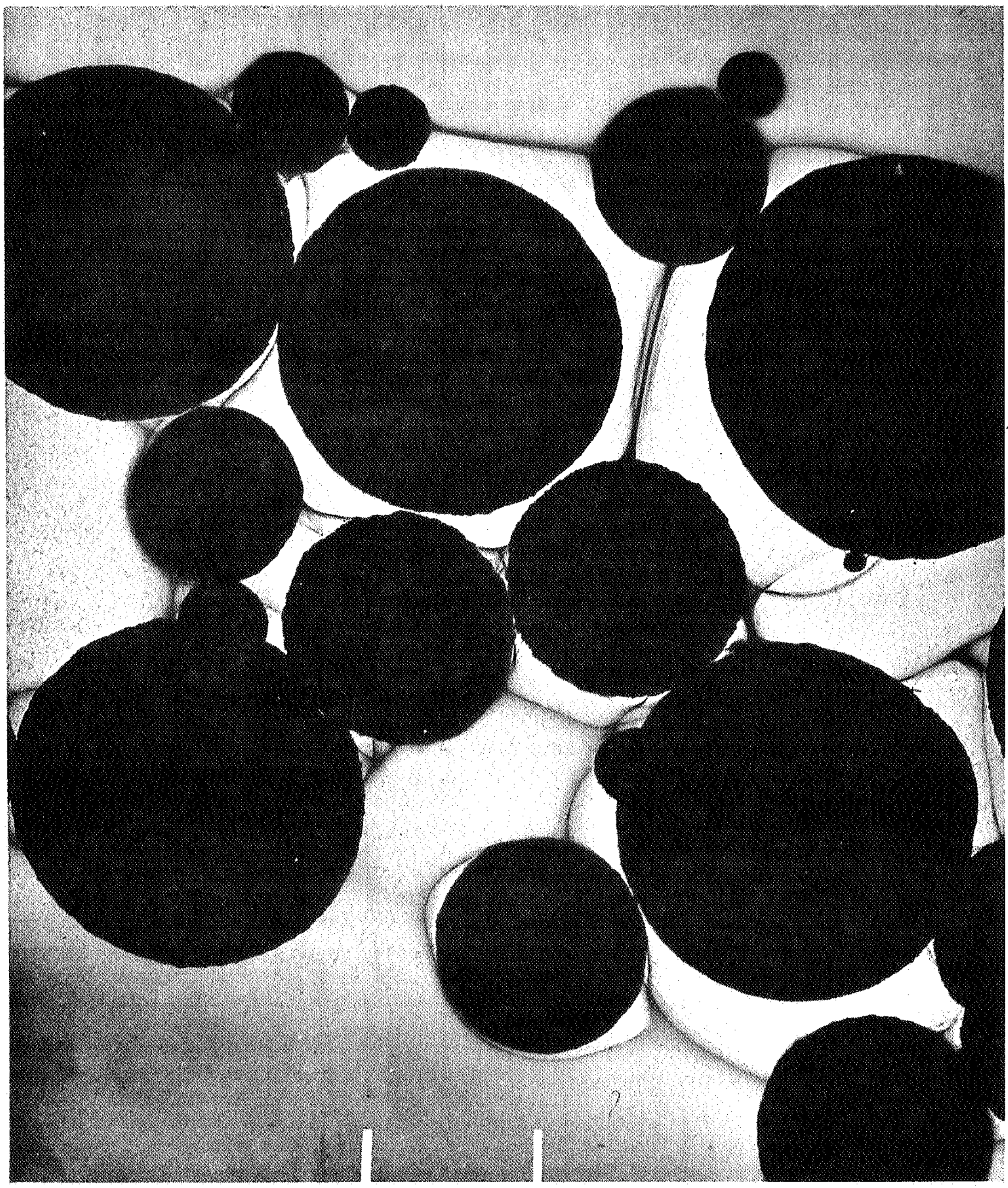

Figure 2. Electron Micrograph of the iron particles used in these experiments. The separation of the index marks corresponds to 1 micron. The background structure is due to the collodion film which supports the particles.

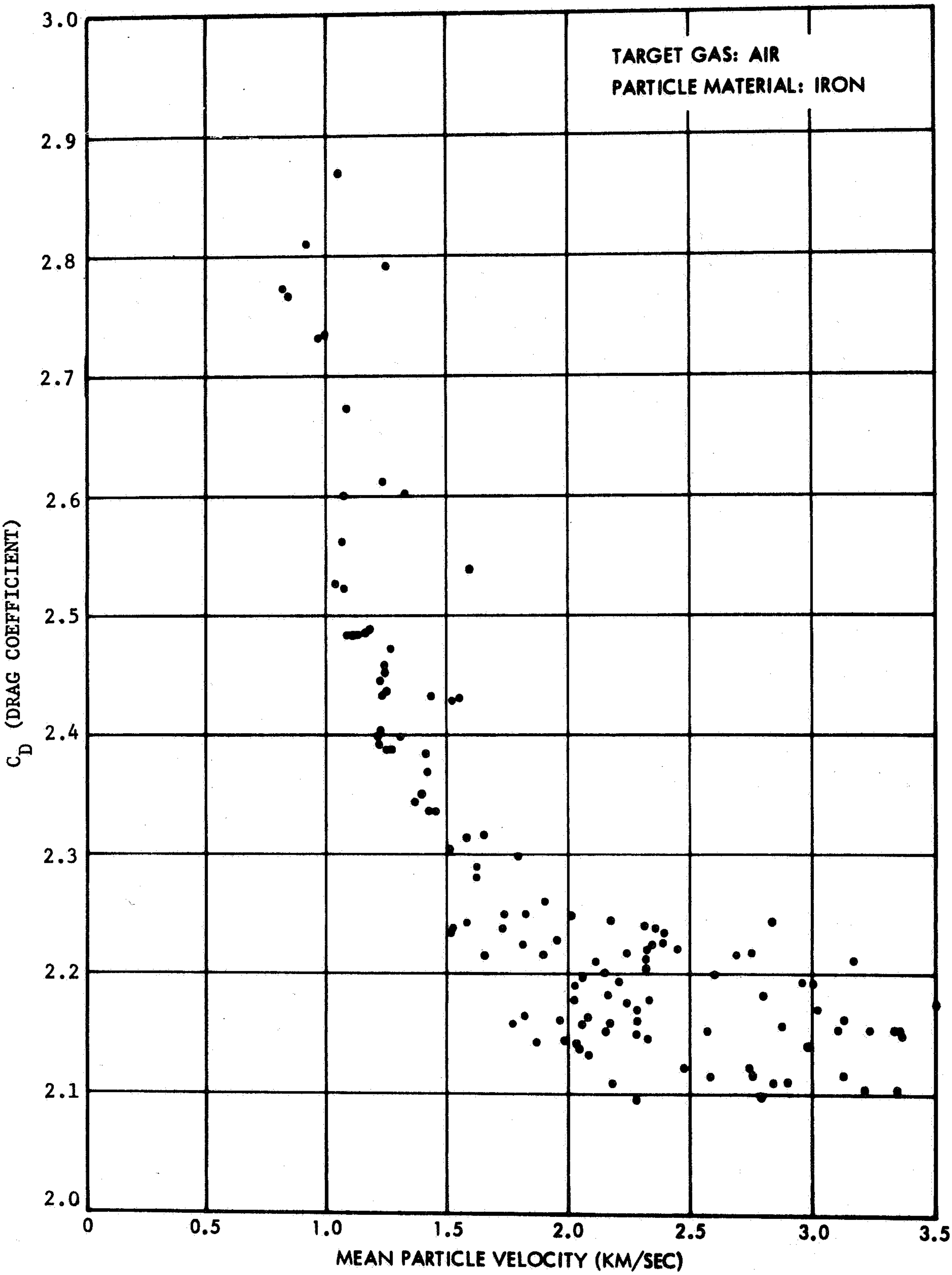

Figure 3. Drag coefficients as a function of average velocity for microscopic iron spheres in free-molecule flow.

changing drag coefficient. Assuming the errors are truly random, average values can be used with a high degree of confidence. The averaging has been accomplished by means of a polynomial least square fit to the data points as illustrated in succeeding sections of this report. The main source of possible systematic error appears to be in the measurement of absolute gas pressure which is estimated to be good to $\pm$ 1%. Other systematic errors include errors in calibrating the charge detector and the total accelerating voltage. These are generally small and the average value of C_D at a given velocity is assumed to be good to $\pm$ 1.5% on an absolute basis.

3. COMPARISON OF THEORY AND EXPERIMENT

3.1 GENERAL

Each experimental data point shown in Figure 3 represents the net momentum transfer from an enormous number of collisions of the target gas with the sphere. One cannot expect to uniquely determine the parameters which describe the behavior of individual molecules interacting with a surface knowing only the drag coefficient. What can be learned, however, is how well current free-molecule drag prediction models compare with the data. Such comparisons may be used to establish the superiority of one model over another or to infer possible modifications of the basic models. The analytical models usually give the drag coefficient as a function of the speed ratio which is defined as the ratio of the velocity of the body to the most probable speed of the background gas, i.e.,

$$S = \frac{V}{\sqrt{2RT}} \tag{9}$$

where T is the (Maxwellian) temperature of the gas and R is the gas constant. The experimental data, expressed in terms of the speed ratio, was fitted to a polynomial curve by the least square method and this curve is utilized for comparison purposes.

3.2 SCHAAF-CHAMBRE MODEL

The Schaaf-Chambre model[2] parameterizes the drag coefficient in terms of σ and σ' which are measures of the exchange of incident normal and tangential momentum, respectively, with the surface of the sphere. Here,

$$\sigma = \frac{P_i - P_r}{P_i - P_w}$$
$$\sigma' = \frac{\tau_i - \tau_r}{\tau_i} \tag{10}$$

where P_i and τ_i are the normal and tangential momentum flux incident on the sphere, respectively, P_r and τ_r are the re-emitted values, and P_w is the normal momentum flux which would be re-emitted if all the molecules were re-emitted in Maxwellian equilibrium with the sphere. The Schaaf-Chambre drag coefficient for a sphere is

$$C_D = \frac{2-\sigma'+\sigma}{2S^2}\left\{\frac{4S^4+4S^2-1}{2S}\,\mathrm{erf}(S) + \frac{(2S^2+1)}{\sqrt{\pi}}\,e^{-S^2}\right\} + \frac{2\sigma'}{3S}\sqrt{\frac{\pi T_w}{T}} \quad . \tag{11}$$

Equation (11) indicates that, for the particular case of spheres, C_D is relatively insensitive to the values of σ or σ' when $\sigma \simeq \sigma'$ (at least for large S and small T_w/T). This is confirmed by Figure 4 where curves corresponding to the cases $\sigma = \sigma' = 1/3$, $\sigma = \sigma' = 1/2$, and $\sigma = \sigma' = 2/3$ are plotted along with the least square polynomial fit to the experimental data. For $S > 3$ all of the curves fall within the range of accuracy of the experimental results. If forced to make a choice, one would likely choose the curve for $\sigma = \sigma' = 1/2$ as the best approximation of the experimental curve over the entire range of speed ratios. However, the scatter exhibited by the experimental data and the insensitivity of the Schaaf-Chambre formulation combine to preclude a positive conclusion.

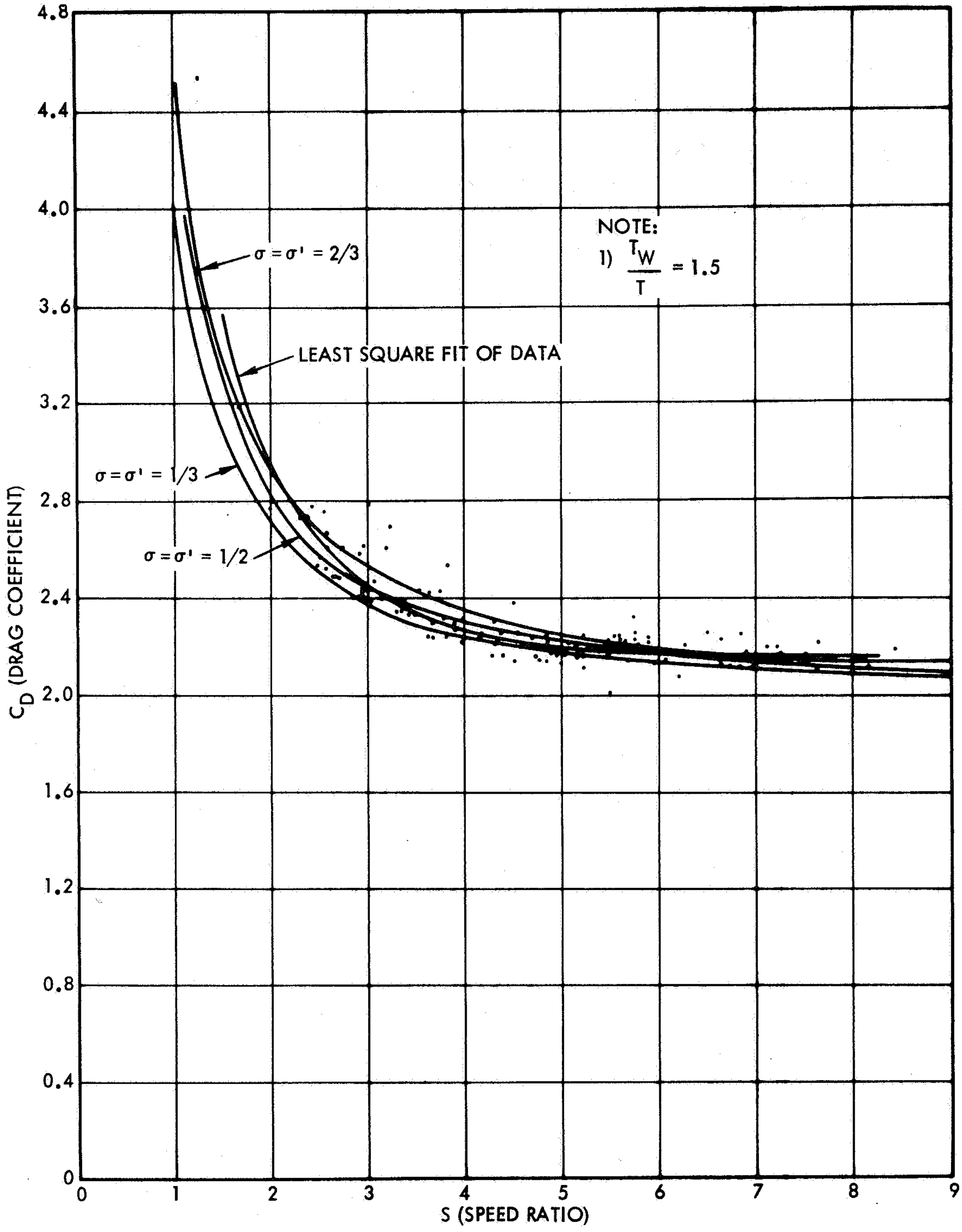

Figure 4. Comparison of the Schaaf-Chambre Model with the experimental results for different values of σ and σ'. The actual data points along with the least squares polynomial are shown.

3.3 SCHAMBERG MODEL

Drag coefficients, based on Schamberg's hyperthermal free-molecule model,[1] have also been compared to the experimental data. In his model, the exchange of incident energy with the surface is characterized by three parameters: ν, which defines the mean reflected angle Θ_r of the emitted molecules in terms of the incident angle Θ_i, i.e., $\cos \Theta_r = (\cos \Theta_i)^{\nu}$; ϕ_o, the angle of a cone centered about Θ_r which contains the re-emitted molecules; and α, the thermal accommodation coefficient. Assuming fully diffuse re-emission (i.e., $\nu = \infty$, $\phi_o = 90°$) and $\alpha = 0.98$, the experimental and predicted drag coefficients are in good agreement for speed ratios in excess of 4, as shown in Figure 5. On the other hand, assuming $\phi_o = 67°$, $\nu = 1.7$, the drag coefficients match for $\alpha = 0.68$. These two examples illustrate the impossibility of uniquely specifying the parameters knowing only the average drag coefficient.

The Schamberg model does not compare well with the data at the lower speed range. This is not surprising, as Schamberg's model treats the incident flow as uniform and parallel (i.e., infinite speed ratio) and corrects for thermal effects by replacing the uniform incident velocity with a Joule gas approximation. In the Joule gas approximation, a superposition of six uniform beams corresponding to the six possible directions of motion of the molecule which compose the Joule gas is assumed.

In an attempt to improve the matching, Schamberg's model has been extended by replacing his incident hyperthermal beam with an incident Maxwellian beam. Extending Schamberg's model to Maxwellian incident flow is equivalent to summing an infinite number of incident monochromatic beams, each weighted by a Maxwellian velocity distribution. A detailed discussion of the modification of Schamberg's model to all speed ranges is presented in the Appendix. Only the results are presented here. The drag coefficient for a sphere is given by the expression

$$C_D = \underbrace{\frac{1}{S^3}\left\{\left(\frac{4S^4+4S^2-1}{2S}\right)\mathrm{erf}(S) + \frac{(2S^2+1)}{\sqrt{\pi}}\,e^{-S^2}\right\}}_{\text{incident drag}} + \underbrace{2\Phi_3(\phi_o)\,\frac{U_r}{U_i}\,J(\nu;S)}_{\substack{\text{re-emitted or}\\ \text{recoil drag}}} \tag{12}$$

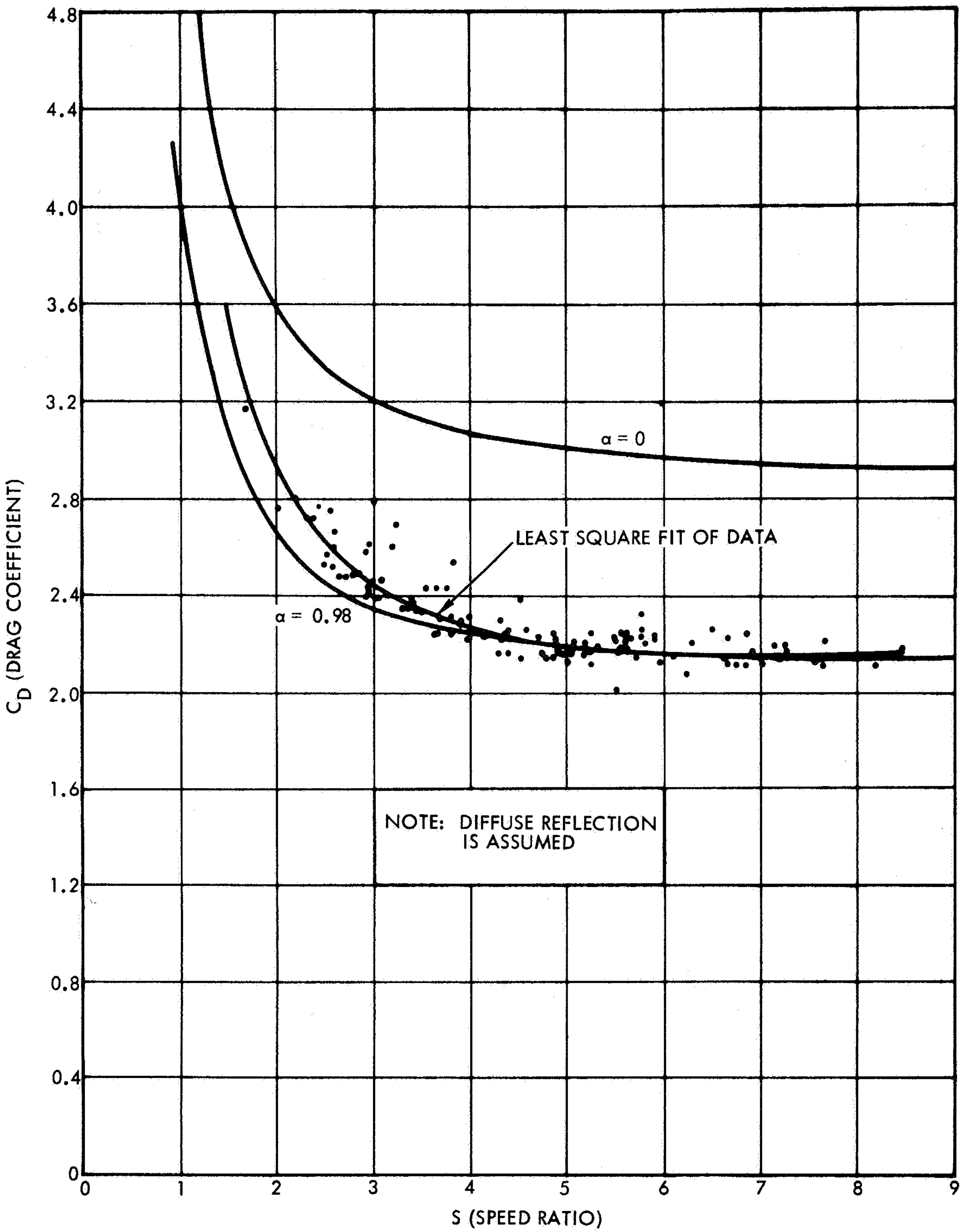

Figure 5. Comparison of Schamberg's hyperthermal model for drag coefficients of spheres in free-molecule flow with the experimental results.

As noted, the first term on the right side of the equation is the contribution due only to the incident molecules while all of the details of the molecule-surface interactions are contained in the second term. As mentioned in the Appendix, this expression reduces to Schamberg's at large speed ratios. Although the modified Schamberg model is based on a somewhat more realistic physical basis, the agreement with experiment is not markedly improved at low speed ratios when values of α and $J(\nu;S)$ are fixed at large speed ratios.

It is likely that the discrepancy between the experimental data and the theoretical model is due to the variation of quantities that are normally assumed to be constant. For example, in comparing the experiment with Schamberg's model, diffuse re-emission and constant accommodation coefficient were assumed. The theoretical curve could be forced to fit the experimental data by adjusting either of these quantities as a function of speed ratio. This need not be an arbitrary adjustment, since a recent theoretical model has been developed by Epstein[3] to predict the behavior of the thermal accommodation coefficient as a function of the speed ratio S for a given surface. His analysis suggests that the thermal accommodation coefficient α behaves as

$$\alpha = \frac{\left(\frac{\varepsilon}{1+\varepsilon}\right)^2 e^{-\frac{S^2}{1+\varepsilon}} \left[\frac{\varepsilon\tau}{\tau+\varepsilon} - \frac{\varepsilon}{1+\varepsilon} + \frac{S^2}{2}\left(\frac{\varepsilon}{1+\varepsilon}\right)^2\right]}{\tau - 1 + 1/2\, S^2} \quad \text{for } \tau > 1 \tag{13}$$

where
$$\varepsilon = \frac{M}{KT}\left(\frac{K\Theta_D d}{h}\right)^2$$
$$\tau = \frac{T_w}{T}$$

Here M is the mass of the incident molecule

K is Boltzmann's constant

Θ_D is the DeBye characteristic temperature

T_w = wall temperature of the solid.

This expression is shown in graphical form in Figure 6 for $\tau = 1.5$ and $\varepsilon = 21.5$.

In order to see if Epstein's model can be used to adjust the theoretical drag coefficient for a better fit to the experimental data, the re-emitted or recoil drag term of Eq. (12) was set equal to the difference between the experimentally measured drag coefficient and the incident drag term, that is

$$2\Phi_3(\phi_o)\,\frac{U_r}{U_i}\,J(\nu;S) = (C_D)_{exp} - \frac{1}{S^3}\left\{\left(\frac{4S^4+4S^2-1}{2S}\right)\text{erg}(S) + \frac{(2S^2+1)}{\sqrt{\pi}}\right\} \tag{14}$$

where $\phi_3(\phi_o)$, U_r/U_i , and $J(\nu;S)$ are defined in the Appendix. From Eq. (14), it can be seen that the quantity $2\Phi_3(\phi_o)$ (U_r/U_i) $J(\nu;S)$ is equal to the difference between the experimentally measured drag coefficient and the drag due only to the incident molecules. U_r/U_i can be evaluated by calculating α from Eq. (13) and assuming values of 1.4 for γ (diatomic gas) and 1.5 for T_w/T_∞ . Furthermore, assuming $\Phi_3(\phi_o) = 2/3$ which corresponds to three dimensional re-emission (see Appendix) leaves $J(\nu;S)$ as the remaining unknown.

A graphical representation of Eq. (14) is shown in Figure 7 which gives a curve representing the least square fit to the data and a curve corresponding to the drag due only to the incident molecules. The difference between the two curves at any value of S is equal to the quantity $2\Phi_3(\phi_o)$ U_r/U_i $J(\nu;S)$ at the same value of S. The value of $J(\nu;S)$ required to force the theoretical curve to match the experimental curve is therefore specified. The relationship between $J(\nu;S)$ and ν is illustrated graphically in Figure 8. In evaluating $J(\nu;S)$ as a function of S and ν, second and higher order terms were neglected which causes some uncertainty for small S and small $J(\nu;S)$. This uncertainty is indicated by the dashed portion of the curve shown in Figure 8. Using the results of Figure 8, the value of ν required to force a fit is shown in Figure 9 as a function of S. Because of the approximation used some uncertainty in the required ν exists for small S. The questionable region is again indicated by the dashed

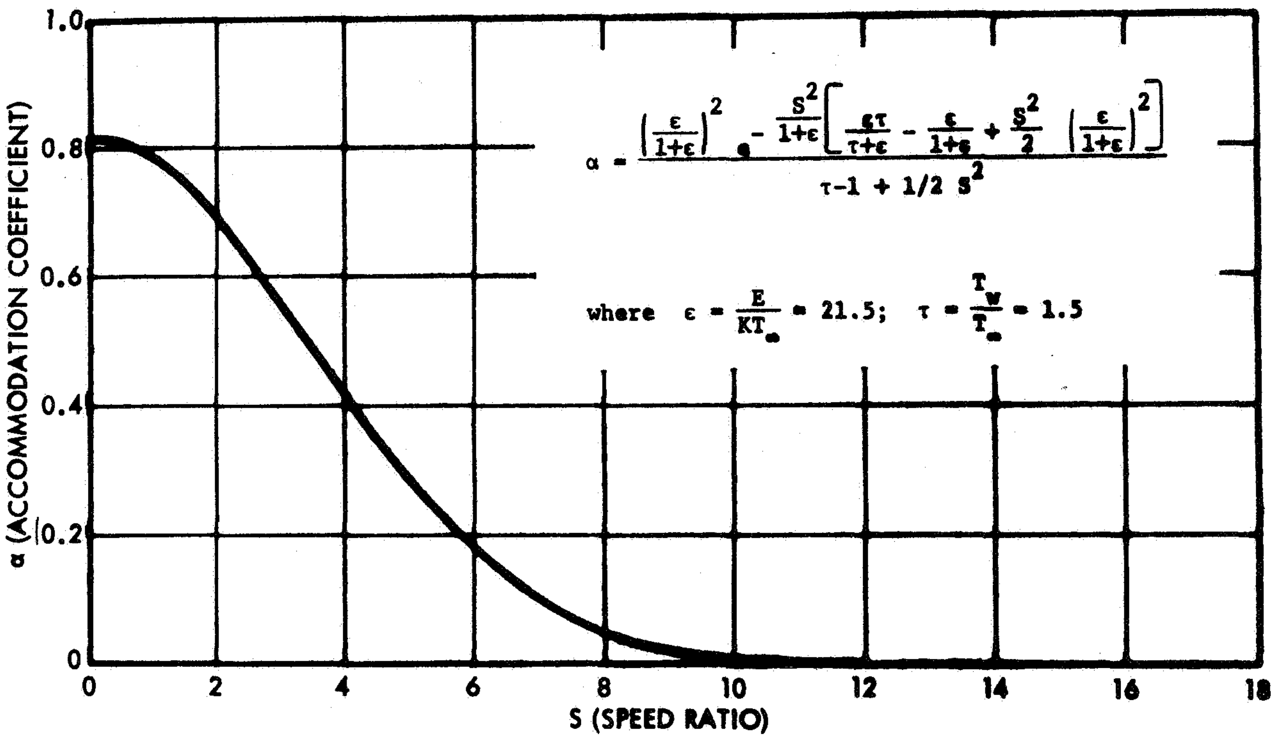

Figure 6. The effect of speed ratio on the thermal accommodation coefficient from Epstein's model.

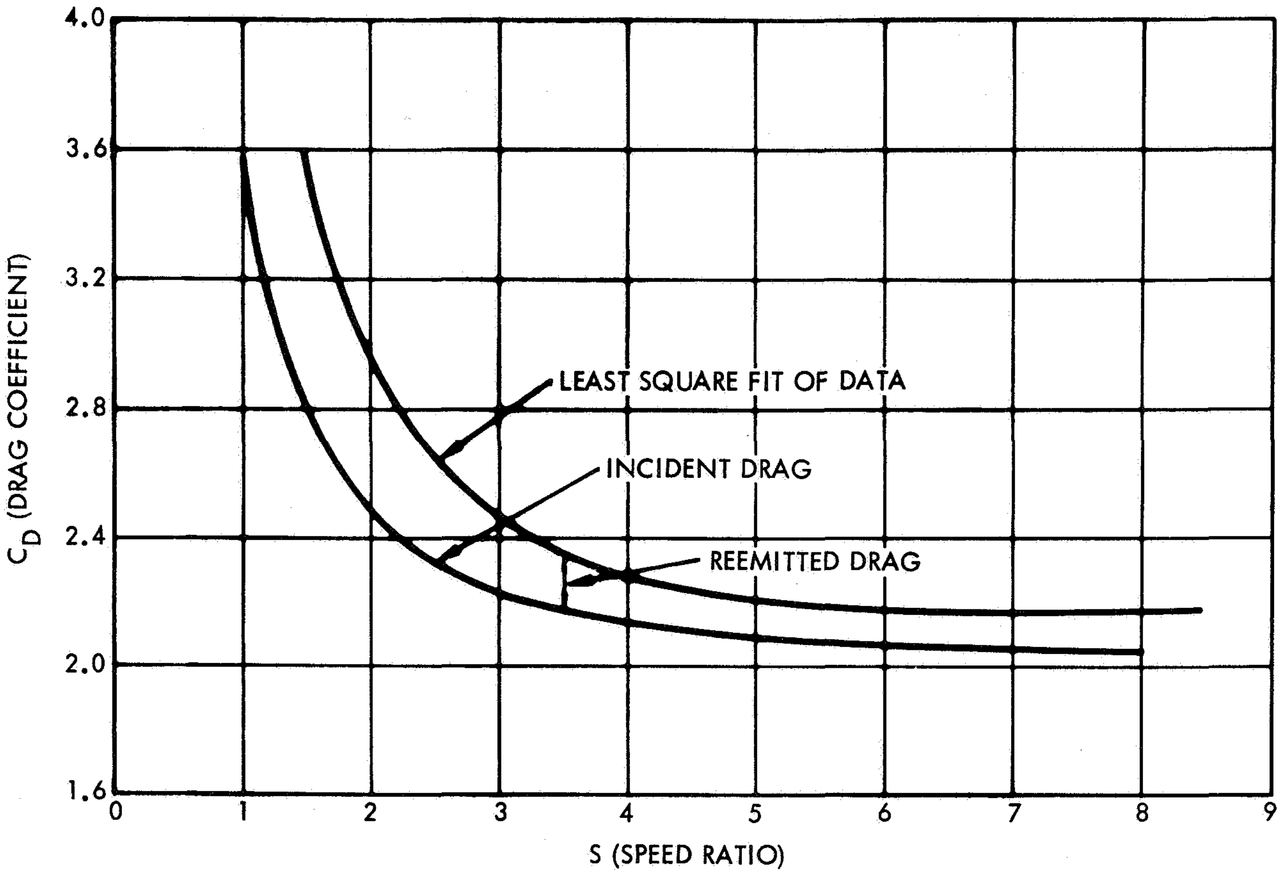

Figure 7. Comparison of the modified Schamberg Model with the experimental results. The curve labeled incident drag represents the contribution to the drag coefficient due only to the incident air molecules. The difference between the curves at any S is attributed to the contribution due only to momentum transferred to the body by the re-emitted molecules.

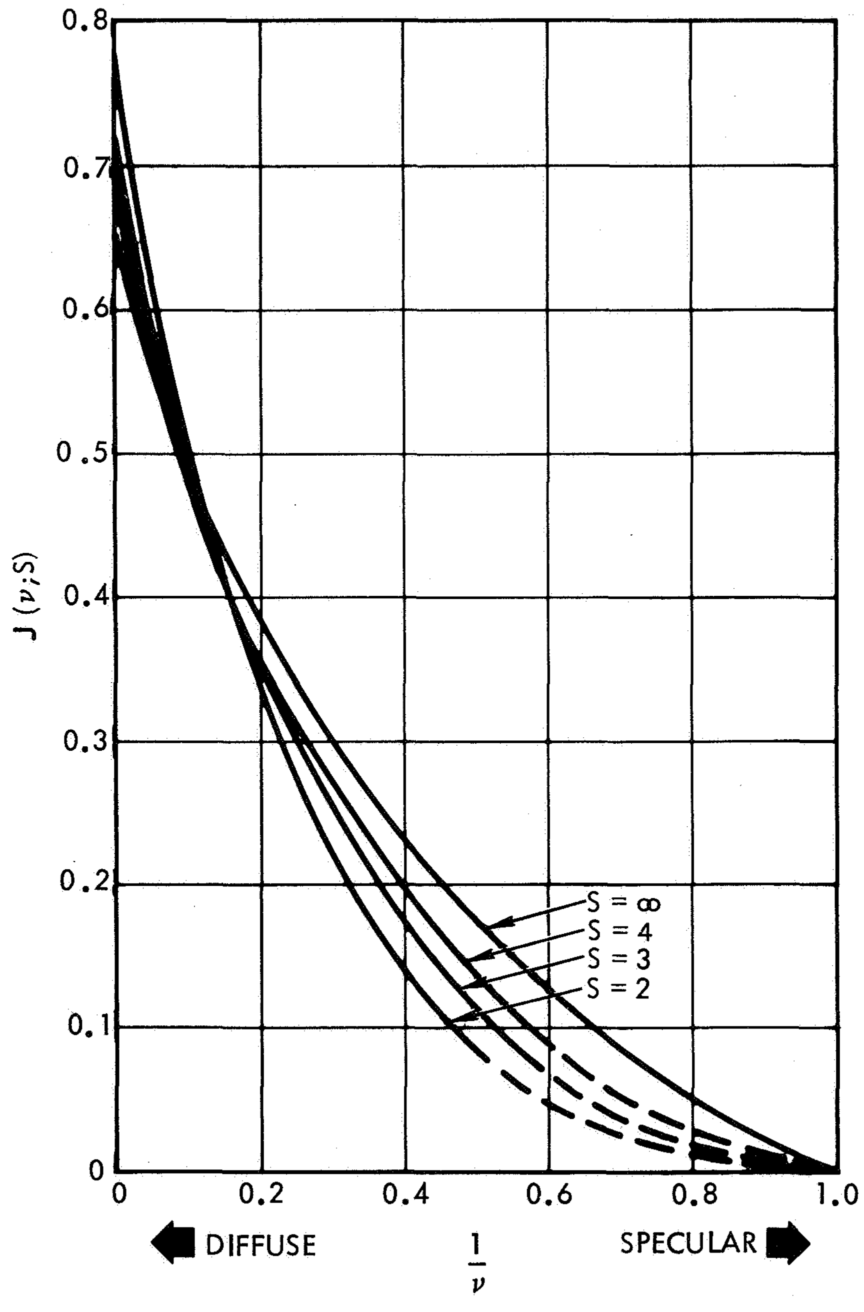

Figure 8. The function of J(ν;S) for a sphere. The S dependence is given by the family of curves labeled for different values of S. The limiting cases of diffuse and specular re-emission are indicated.

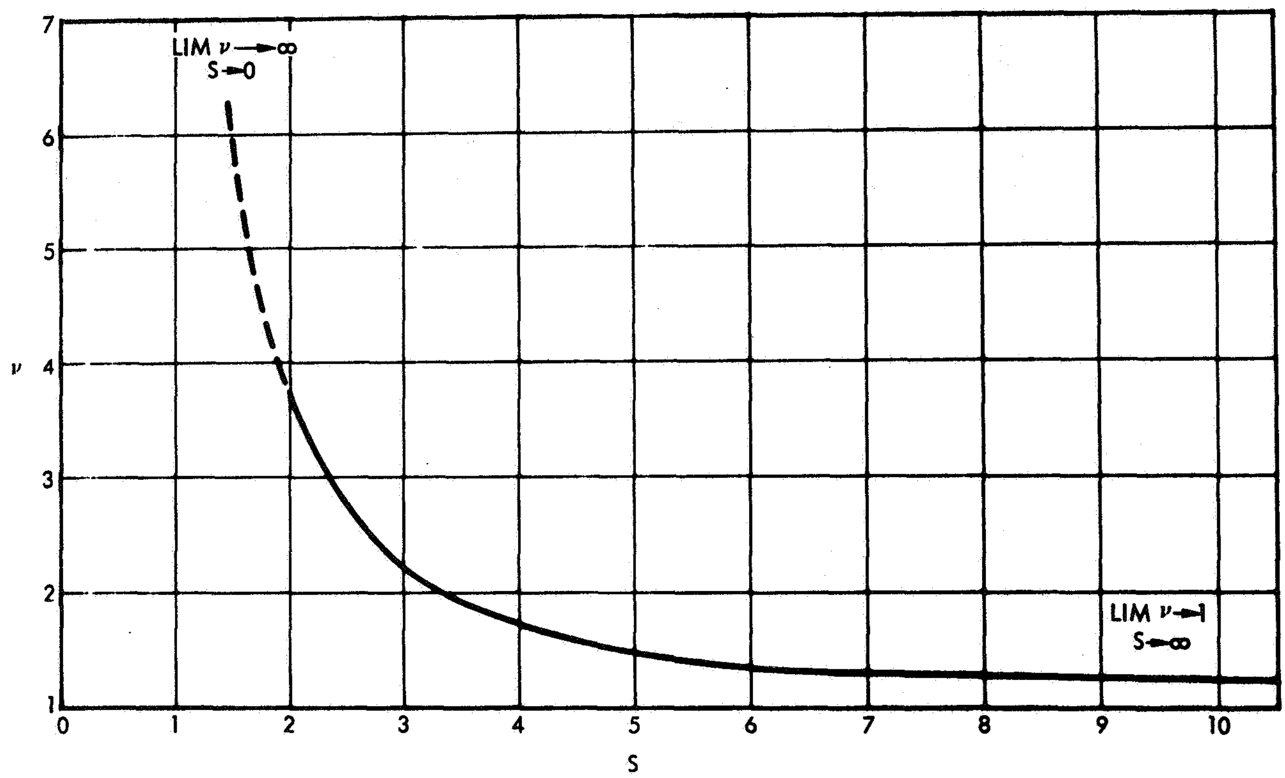

Figure 9. The value of ν as a function of S required to force agreement between the theoretical and experimental curves of Figure 7. Three dimensional reflection is assumed. $\nu = 1$ corresponds to specular reflection while completely diffuse reflection is indicated by $\nu = \infty$.

portion of the curve.

Now $\nu = 1$ corresponds to specular reflection and the implication of Figure 9 is that the collisions become more nearly specular at high speed ratios. When $\nu = \infty$ the re-emission is completely diffuse and again from Figure 9 it appears that $\nu \to \infty$ as $S \to 0$. This result appears to be compatible with the derivation of Epstein since for specular reflection only slight energy accommodation would be expected, i.e., α would approach zero. For lower speed ratios, the molecules tend to reflect diffusely with a large fraction of the energy being accommodated to an energy characteristic of the sphere surface temperature, i.e., α approaches unity.

4. SUMMARY

Average drag coefficients have been measured by the free flight ballistic range technique for microscopic spherical iron particles in a free-molecule environment and the results have been compared to contemporary theories. It has been concluded that a modified version of Schamberg's hyperthermal free-molecule flow model is in better agreement with the experimental data than the Schaaf-Chambre model. The experimental data also provided a framework for testing Epstein's model of the variation of thermal accommodation coefficient with speed ratio. By using the experimental data and the Schamberg and Epstein models, it was found that the atomic collisions must vary from completely elastic at high speed ratios to virtually completely diffuse at low speed ratios. The results provide, of course, only an indirect confirmation of these models. There is not sufficient evidence available to supply an unambiguous solution to the problem. The results which have been obtained, however, constitute a plausible solution.

REFERENCES

1. R. Schamberg, Proceedings of a Symposium on Aerodynamics of the Upper Atmosphere, June 8-10, 1959, Rand Report No. 9-339.

2. S. A. Schaaf and P. L. Chambre, "The Flow of Rarefied Gases", Section H of Fundamentals of Gas Dynamics, H. W. Emmons, ed.

3. M. Epstein, "A Model for the Wall Boundary Condition in Kinetic Theory", Aerospace Report No. TR-669(6240-20)-10, March 1966.

4. J. F. Friichtenicht, Rev. of Sci. Instr., Vol. 33, 209-212 (1962).

5. H. Shelton, C. D. Hendricks, Jr., and R. F. Wuerker, J. Appl. Phys., Vol. 31, 1243-1246 (1960).

6. J. F. Friichtenicht, "Particle Parameter Selection System for an Electrostatic Particle Accelerator", NASA Contractor Report, NASA CR-263, July 1965.

APPENDIX A

DERIVATION OF THE MODIFIED SCHAMBERG MODEL

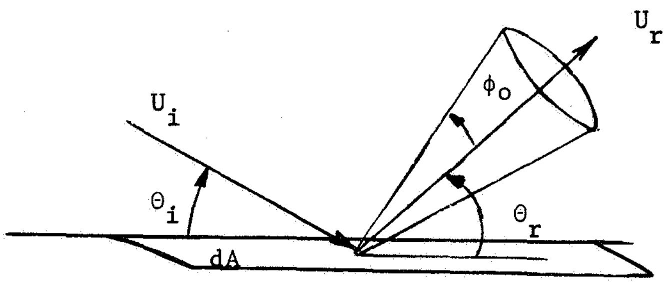

Referring to the figure, the incident particle flux to surface dA is

$$\dot{N}_i = n_\infty \sqrt{\frac{RT}{2\pi}} \left\{ e^{-(S\,\sin\Theta)^2} + \sqrt{\pi}\,(S\,\sin\,\Theta)\left[1+\mathrm{erf}\,(S\,\sin\Theta)\right] \right\} \quad . \tag{1}$$

Let $\dot{n}_r(\omega)$ = number flux of re-emitted particles contained in solid angle between ω and $\omega + d\omega$. Then the number flux of re-emitted particles is given by

$$\dot{N}_r = \int \dot{n}_r(\omega)\, d\omega = \int_0^{\phi_o} 2\pi\, n_r(\phi)\, \sin\phi\, d\phi \quad . \tag{2}$$

Following Schamberg, assume $n_r(\phi) = K \cos \left(\frac{\phi}{\phi_o} \frac{\pi}{2} \right)$. Therefore,

$$\dot{N}_r = 2\pi k \int_0^{\phi_o} \cos \left(\frac{\phi}{\phi_o} \frac{\pi}{2} \right) \sin\phi\, d\phi \quad \text{which yields for } K$$

$$K = \frac{\dot{N}_r}{2\pi} \left\{ \frac{1 - \left(\frac{\pi}{2\phi_o}\right)^2}{1 - \left(\frac{\pi}{2\phi_o}\right) \sin \phi_o} \right\} = \frac{\dot{N}_r}{2\pi} \Phi(\phi_o) \quad . \tag{3}$$

The re-emitted momentum of a single particle about the axis of symmetry (i.e., Θ_r) is computed from the expression

$$M_r (\Theta_r, \phi) = m\, U_r(\phi) \cos\phi \quad . \tag{4}$$

Assume U_r is constant (i.e., is independent of the angle ϕ). The re-emitted momentum flux (i.e., recoil force per unit area) then is

$$F_r(\Theta_r) = \int_0^{\phi_o} M(\Theta_r,\phi)\, n_r(\phi)\, 2\pi \sin\phi\, d\phi = \int_0^{\phi_o} mU_r(\phi) \cos\phi\, 2\pi \sin\phi\, d\phi$$

$$= m\, \dot{N}_r\, U_r\, \Phi(\phi) \cdot \frac{1 - \left(\frac{\pi}{4\phi_o}\right) \sin 2\phi_o}{1 - \left(\frac{\pi}{2\phi_o}\right) \sin\phi_o} \quad .$$

Using Schamberg's notation, let

$$\Phi_3(\phi_o) = (1/4) \times \left[\frac{1 - \left(\frac{\pi}{2\phi_o}\right)^2}{1 - \left(\frac{\pi}{4\phi_o}\right)^2} \right] \left[\frac{1 - \left(\frac{\pi}{4\phi_o}\right) \sin 2\phi_o}{1 - \left(\frac{\pi}{2\phi_o}\right) \sin \phi_o} \right] \quad . \tag{4a}$$

Therefore

$$F_r\ (\Theta_r) = m\ \dot{N}_r\ U_r\ \Phi_3(\phi_o) \quad . \tag{5}$$

Assuming steady state processes, $\dot{N}_r = \dot{N}_i$, Eq. (5) becomes

$$F_r\ (\Theta_r) = m\ \dot{N}_i\ U_r\ \Phi_3(\phi_o) \quad . \tag{5a}$$

To complete the calculations of the re-emitted force per unit area, an expression for U_r, the "average" constant re-emitted velocity, is required.

To calculate U_r, we start from the definition of the thermal accommodation coefficient

$$\alpha = \frac{\dot{E}_i - \dot{E}_r}{\dot{E}_i - \dot{E}_w} = \frac{dE_i - dE_r}{dE_i - dE_w} \tag{6}$$

where

$$dE_i = \frac{1}{2} m\dot{N}_i \left[\underbrace{U_i^2}_{\substack{\text{directed}\\ \text{energy}}} + \underbrace{RT\ (4 + \frac{1}{\phi+1})}_{\substack{\text{translational}\\ \text{energy}}} + \underbrace{\frac{5-3\gamma}{\gamma-1}}_{\substack{\text{internal}\\ \text{energy}}} \right] dA$$

$$dE_r = \frac{1}{2} m\dot{N}_r\ U_r^2$$

$$dE_w = \frac{\gamma+1}{2\ (\gamma-1)}\ mRT_w\ \dot{N}_w \quad .$$

Rewriting dE_i as

$$dE_i = \frac{1}{2} m\dot{N}_i \left[U_i^2 + \left(\frac{\gamma+1}{\gamma-1}\right) RT + \frac{RT}{\phi+1}\right]$$

where

$$\phi = \frac{e^{-(S \sin\Theta)^2}}{\sqrt{\pi}\ (S \sin\Theta)\ [1+\text{erf}\ (S \sin\Theta)]} \quad .$$

Therefore

$$dE_r = dE_i\ (1-\alpha) + \alpha\ dE_w \qquad \text{or}$$

$$\frac{1}{2} m\dot{N}_r\ (U_r^2) = (1-\alpha)\ \frac{1}{2} m\dot{N}_i \left[U_i^2 + \left(\frac{\gamma+1}{\gamma-1}\right)RT + \frac{RT}{\phi+1}\right] + \frac{\alpha}{2} m\dot{N}_w \left(\frac{\gamma+1}{\gamma-1}\right) \quad .$$

From the particle continuity equation, $\dot{N}_r = \dot{N}_i = \dot{N}_w$. Hence, the average re-emitted particle velocity is

$$U_r = U_i \sqrt{(1-\alpha) + \frac{1}{2S^2}\left\{\left(\frac{\gamma+1}{\gamma-1}\right)\left[(1-\alpha) + \alpha\ \frac{T_W}{T}\right] + \frac{(1-\alpha)}{\phi+1}\right\}} \quad . \tag{7}$$

For $S > 1.5$, U_r is approximated as

$$U_r = U_i \sqrt{(1-\alpha) + \frac{1}{2S^2}\left\{\frac{\gamma+1}{\gamma-1}\left[(1-\alpha) + \alpha\frac{T_W}{T}\right] + 1-\alpha\right\}} \quad . \tag{7a}$$

That is, ϕ is set equal to zero. This approximation is reasonable as the experimental data is valid only for $S > 2$.

The re-emitted normal and tangential momentum fluxes are

$$P_r(\Theta) = F_r(\Theta_r)\ \sin\Theta_r \tag{8}$$

$$\tau_r(\Theta) = F_r(\Theta_r)\ \cos\Theta_r \quad .$$

The net pressure and shears on the surface dA is then

$$P = P_i + P_r \tag{9}$$

$$\tau = \tau_i - \tau_r$$

where

$$P_i = \frac{\rho_\infty U_i^2}{2\sqrt{\pi}S^2}\left\{(S\ \sin\Theta)\ e^{-(S\ \sin\Theta)^2} + \sqrt{\pi}\left[\frac{1}{2} + (S\ \sin\Theta)^2\right]\left[1+\text{erf}\ (S\ \sin\Theta)\right]\right\} \tag{10}$$

$$\tau_i = \frac{\rho_\infty U_i^2 \cos\Theta}{2\sqrt{\pi}S}\left\{e^{-(S\ \sin\Theta)^2} + \sqrt{\pi}\ (S\ \sin\Theta)\ \left[1+\text{erf}\ (S\ \sin\Theta)\right]\right\}$$

Inserting these expressions (i.e., (10), (1), (3), (4a), (5), (7a), and (8) into (9) yields:

$$P = \frac{\rho_\infty RT}{\sqrt{\pi}} \left\{ (S \sin\Theta)\, e^{-(S \sin\Theta)} + \sqrt{\pi} \left[\frac{1}{2} + (S \sin\Theta)^2 \right] \left[1+\text{erf}\,(S \sin\Theta) \right] \right\}$$

$$+ \Phi_3(\phi_o)\rho_\infty \sqrt{\frac{RT}{2\pi}} \left\{ e^{-(S \sin\Theta)^2} + \sqrt{\pi} \left[1+\text{erf}\,(S \sin\Theta) \right] \right\} U_r \sqrt{1-(\cos\Theta)^{2\nu}} \tag{11}$$

and

$$\tau = \frac{\rho_\infty U_i^2 \cos\Theta}{2\sqrt{\pi}\, S} \left\{ e^{-(S \sin\Theta)^2} + \sqrt{\pi}\,(S \sin\Theta) \left[1+\text{erf}\,(S \sin\Theta) \right] \right\}$$

$$- U_r \cos^\nu\Theta\, \Phi_3(\phi_o)\, \rho_\infty \sqrt{\frac{RT}{2\pi}} \left\{ e^{-(S \sin\Theta)^2} + \sqrt{\pi}\, (S \sin\Theta) \left[1+\text{erf}\,(S \sin\Theta) \right] \right\} . \tag{12}$$

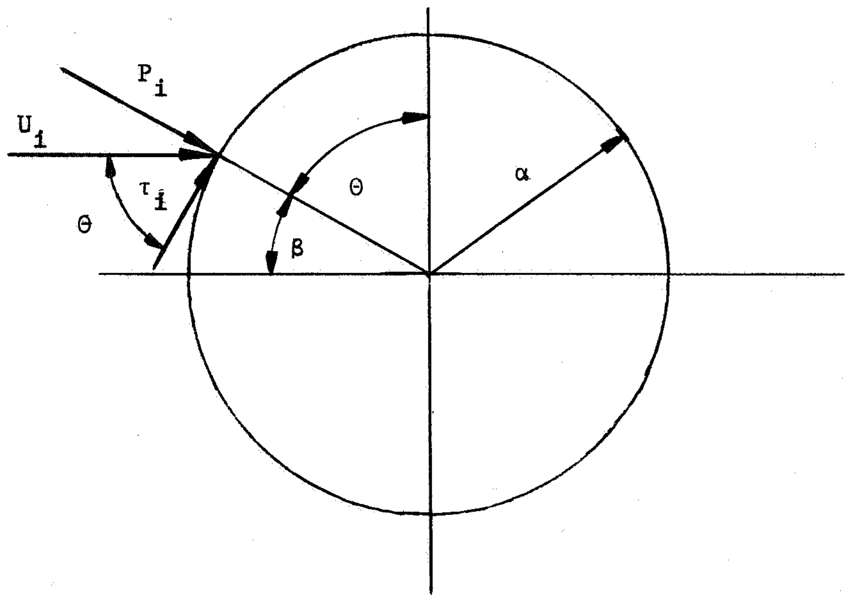

Integrating p and τ over the surface of a sphere where

$$dA = 2\pi a \, (S \sin\beta) \, \alpha d\beta = - 2\pi a^2 \cos\Theta \, d\Theta$$

yields for the drag

$$D = 2\pi a \int_{-\pi/2}^{\pi/2} (P \sin\Theta \cos\Theta + \tau \cos^2\Theta) \, d\Theta \quad .$$

Substituting (11) and (12) yields for the drag

$$D = \frac{\pi a^2 \rho_\infty U_i^2}{\sqrt{\pi} \, S^2} \int_{-\pi/2}^{\pi/2} \left\{ (S \cos\Theta) \, e^{-(S \sin\Theta)^2} + \sqrt{\pi} \, (S^2 + \tfrac{1}{2}) \sin\Theta \cos\Theta \left[1 + \mathrm{erf} \, (S \sin\Theta) \right] \right\} d\Theta$$

$$+ 2\pi a^2 \rho_\infty \frac{RT}{2\pi} \Phi_3(\phi_o) \, \overline{U}_r \int_{-\pi/2}^{\pi/2} \left\{ \left[\sin\Theta \cos\Theta \sqrt{1-(\cos\Theta)^{2\nu}} - (\cos\Theta)^{2+\nu} \right] e^{-(S \sin\Theta)^2} \right.$$

$$\left. + \sqrt{\pi} \, S \left[\sin^2\Theta \cos\Theta \sqrt{1-(\cos\Theta)^{2\nu}} - \sin\Theta \, (\cos\Theta)^{2+\nu} \right] \left[1 + \mathrm{erf} \, (S \sin\Theta) \right] \right\} d\Theta$$

Integrating yields

$$D = \frac{\pi a^2 \rho_\infty U_i^2}{2S^3} \left\{ \frac{4S^4 + 4S^2 - 1}{2S} \operatorname{erf}(S) + \frac{(2S^2 + 1)}{\sqrt{\pi}} \; e^{-S^2} \right\}$$

$$+ 2\pi a^2 \rho_\infty U_r \sqrt{\frac{RT}{2}} \, \Phi_3(\phi_o) \left[I_1(\nu;S) + \sqrt{\pi} S \left[I_2(\nu) + I_3(\nu;S) \right] \right]$$

where

$$I_1(\nu;S) = \int_{-\pi/2}^{\pi/2} \left[\sin\Theta \cos\Theta \sqrt{1-(\cos\Theta)^{2\nu}} - (\cos\Theta)^{2+\nu} \right] e^{-(S \sin\Theta)^2} \, d\Theta$$

$$I_2(\nu) = \int_{-\pi/2}^{\pi/2} \left[\sin^2\Theta \cos\Theta \sqrt{1-(\cos\Theta)^{2\nu}} - \sin\Theta \, (\cos\Theta)^{2+\nu} \right] d\Theta$$

$$I_3(\nu;S) = \int_{-\pi/2}^{\pi/2} \left[\sin^2\Theta \cos\Theta \sqrt{1-(\cos\Theta)^{2\nu}} - \sin\Theta \, (\cos\Theta)^{2+\nu} \right] \operatorname{erf}(S \sin\Theta) \, d\Theta \quad .$$

An accurate integration of the integrals $I_1(\nu;S)$, $I_2(\nu)$, and $I_3(\nu;S)$ valid for all speed ratios requires an extensive effort and this exercise has not been carried out. However, the experimental data includes only speed ratios greater than two and for S in excess of two reasonable approximations are to set $\mathrm{erf}(S) \simeq 1$ and $e^{-S^2} \cong 0$. With these approximations,

$$I_1(\nu;S) \cong \begin{cases} -\frac{\sqrt{\pi}}{S}\left(1-\frac{\nu+1}{4S^2}\right) & \text{for } \nu < 4S^2-1 \\ & \text{for } \nu \geq 4S^2-1 \end{cases}$$

and,

$$I_3(\nu;S) \cong \frac{-2}{\nu+3} + \frac{1}{2S^2}\left(1-\frac{3}{4S^2}\right) \quad .$$

Defining $I(\nu;S) = I_1(\nu;S) + \sqrt{\pi}S\left[I_2(\nu) + I_3(\nu;S)\right]$, then

$$J(\nu;S) = \frac{I(\nu;S)}{\sqrt{\pi}\ S} \cong -\frac{1}{S^2}\left(1-\frac{\nu+1}{4S^2}\right) + f(\nu) + \frac{1}{2S^2}\left(1-\frac{3}{4S^2}\right)$$

where $f(\nu) = 2\left\{I_2(\nu) - \frac{1}{\nu+3}\right\}$ is tabulated in Schamberg's report.

Introducing the drag coefficient $C_D = \dfrac{D}{1/2\ \rho_\infty(\pi a^2)U_i^2}$

$$C_D = \frac{1}{S^2}\left\{\left[\frac{4S^4+4S^2-1}{2S}\right]\mathrm{erf}(S) + \frac{(2S^2+1)}{\sqrt{\pi}}\ e^{-S^2}\right\} + 2\Phi_3(\phi_o)\ \frac{U_r}{U_i}\ J\ (\nu;S) \quad . \qquad (13)$$

For large S, fully diffuse re-emission, and a three-dimensional conical beam

$$J(\nu \to \infty;\ S \to \infty) = 2/3$$

$$\Phi_3(\phi_o = 90°) = 2/3$$

$$\frac{U_r}{U_i} = \sqrt{1-\alpha} \quad .$$

Then in the limit as $S \to \infty$, $\nu \to \infty$, and $\phi_o \to 90°$,

$$C_D = 2 + \frac{8}{9}\sqrt{1-\alpha}$$

which is in agreement with Schamberg.

NASA-Langley, 1967 —— 1 CR-776